




# DEVELOPMENT OF ATOMIC LAYER DEPOSITION HEMOCOMPATIBLE COATINGS FOR MATERIALS DEDICATED FOR THE IMPLANTS IN THE CARDIOVASCULAR ENVIRONMENT

KAROLINA SZAWIRAACZ<sup>1\*</sup> , PRZEMYSŁAW KURTYKA<sup>1,2</sup> , JUSTYNA WIĘCEK-CHMIELARZ<sup>1</sup> , ZUZANNA ZAJĄC<sup>1,3</sup> , MARCIN BASIAGA<sup>4</sup> , ANNA TARATUTA<sup>4</sup> , ROMAN OSTROWSKI<sup>5</sup> , ROMAN MAJOR<sup>1\*</sup> 

<sup>1</sup> INSTITUTE OF METALLURGY AND MATERIALS SCIENCE, POLISH ACADEMY OF SCIENCES, 25 REYMONTA ST., 30-059 KRAKOW, POLAND

<sup>2</sup> FOUNDATION OF CARDIAC SURGERY DEVELOPMENT, INSTITUTE OF HEART PROSTHESES, 345A WOLNOŚCI ST., 41-800 ZABRZE, POLAND

<sup>3</sup> DEPARTMENT OF EXPERIMENTAL MECHANICS AND BIOMECHANICS, FACULTY OF MECHANICAL ENGINEERING, CRACOW UNIVERSITY OF TECHNOLOGY, 37 JANA PAWŁA II AV., 31-864 KRAKOW, POLAND

<sup>4</sup> DEPARTMENT OF BIOMATERIALS AND MEDICAL DEVICES ENGINEERING, FACULTY OF BIOMEDICAL ENGINEERING, SILESIA UNIVERSITY OF TECHNOLOGY, ROOSEVELTA 40 ST., ZABRZE 41-800, POLAND

<sup>5</sup> INSTITUTE OF OPTOELECTRONICS, MILITARY UNIVERSITY OF TECHNOLOGY IN WARSAW, 2 GEN. S. KALISKIEGO STR., 00-908 WARSAW, POLAND

\*E-MAIL: SZAWIRAACZ.K@IMIM.PL; MAJOR.R@IMIM.PL

## Abstract

*An atrial septal defect (ASD) is one of the most common congenital heart defects in children and the most frequent congenital defect found in adults. Currently, several types of kits are available for percutaneous closure of ASD. The design of these implants is based on the Nitinol alloy. Despite the good biocompatibility of Nitinol alloys, the use of these materials for long-term implantation is questionable due to the high nickel content and the risk of releasing nickel ions as a result of corrosion in the body's environment. A way to improve the hemocompatibility of Nitinol alloys is to modify their surface. As part of this work, the conditions for the production of SiO<sub>2</sub> surface layers using the atomic layer deposition (ALD) method and laser surface modification with three different laser cutting speeds were developed to improve biocompatibility. This allowed us for the comparison of different surface modifications (ALD and laser modification) in terms of their impact on cell-material interactions. The general analysis concerning biocompatibility confirmed the biological usability of the designed ALD deposited coatings. Surface nanostructuring had a positive effect on the natural biological layer formation.*

[Engineering of Biomaterials 172 (2024) 06]

doi:10.34821/eng.biomat.172.2024.06

Submitted: 2024-07-18, Accepted: 2024-08-08, Published: 2024-08-12



Copyright © 2024 by the authors. Some rights reserved. Except otherwise noted, this work is licensed under <https://creativecommons.org/licenses/by/4.0>

*The analysis performed indicated the appropriate behaviour of the natural biological layer, known in the literature as pseudointima, in contact with blood. It was evident that platelet activation on the surface was reduced.*

**Keywords:** Nitinol alloys, biocompatibility, hemocompatibility, cytotoxicity, protein adsorption, coagulation system activation

## Introduction

Cardiovascular diseases, in particular congenital heart defects, are increasingly being diagnosed in children and adults. One of the most common congenital defects is the atrial septal defect (ASD). In this condition, there is a hole in the atrium between the upper heart chambers. As a result, some oxygenated blood flows through the hole, where it mixes with oxygen-poor blood and increases the total amount of blood that flows toward the lungs [1,2].

Several types of closure devices and tools are currently available. One of the most frequently used is the self-expanding, product of Abbot, Amplatzer Septal Occluder set [3].

The design of these implants is based on the Nitinol. This alloy of nickel and titanium with shape memory and superelasticity is used in medicine, especially in vascular and orthopaedic implants, due to its biocompatibility and flexibility. The implant has a wide waist that centers the device and fills the hole. The transcatheter delivery makes it the proven standard of care for the occlusion of ASDs [3-5].

Nitinol is frequently used in the production of medical implants due to its beneficial properties, such as biocompatibility and resistance to material fatigue. Nitinol stands out in particular, recognized as the best in terms of hemocompatibility – the material's ability to contact blood without causing negative effects, such as blood cell damage, protein adsorption, or platelet aggregation, which could lead to the formation of blood clots [6].

However, despite its general biocompatibility, the use of the Nitinol alloy carries certain risks. Potential complications include allergic reactions caused by the release of nickel ions, excessive overgrowth of the implant with endothelial tissue, and the possibility of blood clot formation on the implant surface [4,6].

The effectiveness of implants made of Nitinol depends mainly on the physicochemical properties of their surface. Therefore, current research focuses on developing the surface in the form of thin coatings as well as nanostructuring that could significantly reduce the blood clotting process and provide better biotolerance in the cardiovascular environment [7-9].

This work concerns surface modification of Nitinol substrate by atomic layer deposition (ALD) process and with laser nanostructuring. By implanting textured surfaces in contact with blood, a set of cascade reactions occurs leading to formation of a natural protein layer constituting a natural barrier between the material and the blood, effectively inhibiting its activation [10-13].

## Materials and Methods

### Surface modification

The Nitinol surface was modified with  $\text{SiO}_2$  layers using the ALD method. Discs with a diameter of 14 mm were laser-cut from a 0.8 mm thick Nitinol sheet supplied by Wolften Sp. z o.o. and utilized for testing. This is a standard sample size used in the laboratory due to its compatibility with the equipment available for testing. The chemical composition and mechanical properties of the materials tested met the requirements outlined in the ASTM F2063-18 standard. The final austenite temperature ( $A_f$ ) was below  $15^\circ\text{C}$ . Before coating, the surface of the Nitinol alloy underwent electrochemical polishing. This process led to surface passivation due to the type of solution used during electrochemical polishing. All samples were then cleaned in an ultrasonic bath for 10 min at  $20^\circ\text{C}$  in 96% ethyl alcohol.

In the next step, a thin layer of  $\text{SiO}_2$  was applied using the ALD technique, utilizing heated tetramethoxysilane, 98% and water ( $\text{H}_2\text{O}$ ) as the precursors. Most coating techniques require high temperatures, which could cause equilibrium phases formation such as  $\text{Ni}_3\text{Ti}$  and  $\text{Ti}_2\text{Ni}$ , or non-equilibrium phases unrelated to the shape memory effect. These phases can negatively impact the substrate properties. Therefore, it was critical to employ low-temperature surface modification techniques for Nitinol alloys. The ALD process was carried out at  $200^\circ\text{C}$ . High-purity nitrogen 5.0 ( $\text{N}_2$ ) was used as both a carrier and a purge gas, with a flow rate of  $200\text{ cm}^3/\text{min}$  for the precursor and water. Nitrogen 5.0 denotes nitrogen with 99.999% purity, used to minimize contamination during the process. The sample set was divided into two groups: one without a coating and one with 1000 ALD cycles of  $\text{SiO}_2$ .

The final step in sample preparation was sterilization in an autoclave at  $135^\circ\text{C}$  and 2.1 bar pressure to eliminate any microorganisms from the surface before further testing. To maintain consistency in presenting test results, the following labels were used:

- Nitinol: samples made from Nitinol alloy,
- Nitinol +  $\text{SiO}_2$ : samples with a  $\text{SiO}_2$  coating on the Nitinol alloy.

Simultaneously, to assess the influence of surface topography on cell response, a laser modification was performed. This allowed us for the comparison of different surface modifications (ALD and laser modification) in terms of their impact on cell-material interactions. This approach enabled a better understanding of how surface topography, independent of material chemistry, can affect biocompatibility.

Such an approach facilitates a comparison of both techniques and their outcomes, emphasizing the role of both chemical composition and topography in evaluating the properties of biomaterials.

To enhance the protein adsorption potential, the surface was nanostructured using a picosecond laser. Laser surface nanostructuring involved the precise modification of the material's surface topography through the application of short, high-energy laser pulses. This process entailed the controlled interaction of the laser beam with the material's surface, leading to the formation of nanostructures with varying topographies. When the laser beam interacted with the surface, it caused localized, rapid heating, melting, and evaporation of the material, resulting in the formation of nanometer-scale structures. The laser-based process allowed for the creation of complex surface patterns that increased roughness and active surface area, which could improve the adhesive properties. Laser parameters such as pulse energy, repetition rate, and exposure time were optimized to produce structures influencing on protein adsorption.

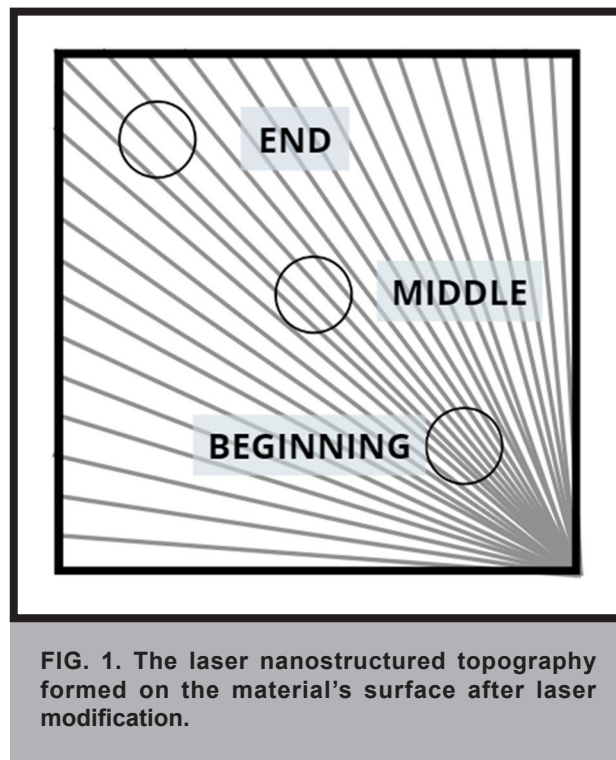


FIG. 1. The laser nanostructured topography formed on the material's surface after laser modification.

The structures were prepared as radially spreading lines in the form of channels. The described approach to nanostructuring of the surface made it possible to select the optimal distance from the "valleys" on the formed topography (FIG. 1). The sample's surface featured areas where the channels were farthest apart (END), areas where the channels were spaced at an average distance (MIDDLE), and areas where the channels were positioned closest together (BEGINNING). The observation points (END, MIDDLE, BEGINNING) were adopted conventionally. The aim of these observations was to provide a general assessment of how cell behaviour changes with varying distances between the valleys on the formed topography.

A picosecond laser PL 2210/SH/TH/FH from Ekspla was used during the grooving process. The fixed parameters of the laser radiation were as follows: wavelength  $\lambda = 355\text{ nm}$ , pulse duration  $\tau_i = 70\text{ ps}$ , repetition rate  $f_p = 1\text{ kHz}$ . The pulse energy was varied using an external Variable Attenuator 355 nm from Eksma. A galvanometric scanner SS-IIE-10 [TY] from Raylase with a F-theta lens S4LFT4010/126 from Sill Optics with a focal length of  $f = 163\text{ mm}$  was used in the setup. The scanner was controlled by WeldMARK 2.0 software from Raylase. The grooving process was conducted at scanning speeds of  $2\text{ mm/s}$ ,  $6\text{ mm/s}$ ,  $8\text{ mm/s}$ , and  $10\text{ mm/s}$ . Each successive groove on the sample was angled  $1^\circ$  relative to the previous one. A list of the prepared samples is presented in TABLE 1. The thickness of the coating was estimated based on gas flow and time of deposition, sccm means standard cubic cm per minute. To deposit the coating using the pulsed magnetron sputtering SPU method of  $15\text{ nm}$  in thickness, a deposition time of  $5\text{ s}$  was needed. To deposit  $118.5\text{ nm}$  coating deposition time was  $40\text{ s}$ . Individual layers were obtained by ablating a Si target (99.99%) and controlling the flow of acetylene, nitrogen and argon, as well as the deposition time.

TABLE 2 presents a list of samples after laser nanostructuring along with the types of analyses conducted to assess their properties.

**TABLE 1. List of samples made using laser nanostructuring by pulsed magnetron sputtering (SPU).**

| Number  | Material | Coating thickness [nm] | Ar + C <sub>2</sub> H <sub>2</sub> Gas flow [sccm] | Scan speed [mm/s] | Pulse energy [ $\mu$ J] |
|---------|----------|------------------------|--|-------------------|-------------------------|
| B372_26 | Si-a-C:H | 15                     | 27 + 3   | 8                 | 6.1 – 6.5               |
|         |          |                        |  | 6                 | 6.1 – 6.5               |
|         |          |                        |  | 2                 | 6.1 – 6.5               |
| B372_29 | Si-a-C:H | 118.5                  | 18 + 12  | 10                | 6.1 – 6.4               |
|         |          |                        |  | 2                 | 6.1 – 6.6               |

**TABLE 2. Samples and types of analyses conducted.**

| Sample          | Type of analysis                               |
|-----------------|--|
| B372_26 2 mm/s  | Hemocompatibility on whole human blood         |
| B372_26 6 mm/s  |  |
| B372_26 8 mm/s  |  |
| B372_29 2 mm/s  | Cell growth on Normal Human Dermal Fibroblasts |
| B372_29 10 mm/s |  |

### Surface topography

After performing surface modifications (ALD), the samples were analysed for surface topography. The studies were conducted using a SmartZoom 5 digital microscope. The images were taken at magnifications of 100 x, 300 x, and 600 x for each sample. Coaxial brightness lighting mode was used.

The Confomap software allows for detailed analysis of surface topography, enabling the measurement of surface roughness, visualization of 3D surface profiles, and evaluation of changes in surface features after modifications such as laser processing. Using the ConfoMap software, the changes in topography that occurred after the creation of channels in the laser-nanostructured samples were analysed. Images of the sample were taken for different cutting speeds of the channels using laser nanostructuring. For samples subjected to laser nanostructuring, analyses of topography were carried out at the three marked locations in the diagram (FIG. 1).

### Analysis of surface wettability

The materials after ALD were evaluated for their contact angle, allowing the assessment of their properties in the context of biomedical applications. In the first stage of the research, the following materials were examined:

- Nitinol substrate;
- Nitinol substrate with ALD deposited coating.

After analysing the contact angle values and surface free energy (SFE), the samples were subjected to protein adsorption on their surface to examine the change in contact angle and SFE depending on the adsorbed protein layer on their surface. For this purpose, the following samples were tested:

- Nitinol – after incubation in fetal bovine serum (FBS) for 48 h;
- Nitinol + ALD coating – after incubation in FBS for 48 h.

The wettability of the test samples was measured using the Drop Shape Analyser DSA100 optical goniometer (KRÜSS, Germany) together with the DSA4 computer program. Distilled water, phosphate-buffered saline (PBS), diiodomethane and 10 X FBS were used as measuring fluids. Experiments utilized a 10 X concentrated FBS solution, prepared to achieve a tenfold higher nutrient concentration compared to standard 10% FBS, which corresponds to pure FBS.

Standardised liquids for measuring the contact angle, according to ASTM D7334 standard, are water and diiodomethane. In this case, we additionally used PBS and FBS because these liquids were applied to simulate biological conditions. This allows the assessment of how the material behaves in an environment that reflects physiological conditions, which is crucial for understanding its potential biocompatibility. The size of the measuring droplet deposited on the material was 5  $\mu$ L. Based on the results obtained, the SFE was determined using the Owens-Wendt method.

### Biological assessment

The biocompatibility of the modified surfaces was done using cell culture models, which included cytotoxicity testing according to the PN-EN ISO 10993-5 standard on the samples after ALD surface modification. The biocompatibility of the ALD deposited SiO<sub>2</sub> was determined by direct cytotoxicity tests as well as by indirect cytotoxicity test, on extracts according to the PN-EN ISO 10993-5 standard with a basic incubation time of 24 h. Tests lasting 48 h were planned to confirm the stability of the material and the validity of the observations made. Cell viability was assessed after 48 h incubation of human fibroblasts with tested materials using confocal microscopy (Carl Zeiss Exciter 5 scanning confocal microscope, Carl Zeiss, Jena, Germany). In brief, human dermal fibroblasts (PromoCell C-12302, PromoCell, Heidelberg, Germany) were seeded in a density of  $0.05 \times 10^6$  cells/well in full growth medium (Fibroblast Growth Medium 2, Promocell) on tested materials (discs with a diameter of 14 mm and a thickness of 0.8 mm) in 24-well plates and cultured for 24 h. The cell culture supernatant was then collected, centrifuged (500g  $\times$  10 min) and stored ( $-80^\circ\text{C}$ ) for evaluation of lactate dehydrogenase (LDH, CytoTox 96@ Non-Radioactive Cytotoxicity Assay, G1780, Promega Corporation, Madison, WI, USA), fluorescein tetraacetate (FDA, MitoTracker™ Green FM, Invitrogen™, Waltham, MA, USA) levels and propidium iodide (PI) staining (Sigma Aldrich, St. Louis, MO, USA) for measurements of cells' viability.

In direct cytotoxicity tests, cells were seeded onto specific samples (discs with a diameter of 14 mm and a thickness of 0.8 mm). In the experiments, cells were used at a concentration of  $7.60 \times 10^7$  per mL. For each sample, 2 mL of cell suspension was added, resulting in  $1.52 \times 10^8$  cells per sample. After 48 h, the supernatant medium above the sample was collected and then tested for LDH enzyme content.

The cells adhering to the material samples were stained using FDA labelling active mitochondria indicating living cells and PI labelling dead, necrotic cells.

After staining the samples were observed using a confocal laser scanning microscope (CLSM Exciter 5 AxioImager, Zeiss). The confocal microscope enables the acquisition of high-resolution fluorescent images with the precise separation of signals from different layers of the sample. This allows for the generation of three-dimensional images of the distribution of dead and live cells on the Nitinol surface. Confocal laser microscopy also facilitates accurate quantitative counting of cells and analysis of their distribution on the material's surface.



The second method considered extracts. The material samples were placed in pure medium for 24 h. In this case, the medium from above the samples was mixed with pure cell medium in the following ratio:

- 1 mL of medium from above the sample (10:0);
- 0.9 mL of sample extract and 0.1 mL of pure medium (9:1);
- 0.8 mL of sample extract and 0.2 mL of pure medium (8:2);
- 0.7 mL of sample extract and 0.3 mL of pure medium (7:3);
- 0.6 mL of sample extract and 0.4 mL of pure medium (6:4);
- 0.5 mL of sample extract and 0.5 mL of pure medium (5:5);
- 0.4 mL of sample extract and 0.6 mL of pure medium (4:6);
- 0.3 mL of sample extract and 0.7 mL of pure medium (3:7);
- 0.2 mL of sample extract and 0.8 mL of pure medium (2:8);
- 0.1 mL of sample extract and 0.9 mL of pure medium (1:9);
- 1 mL pure medium (0:10).

The prepared solutions were then placed in a culture vessel and in an incubator (37°C, 5% CO<sub>2</sub>), and after 24 and 48 h, the supernatant was collected into 2 mL Eppendorf tubes and centrifuged (5 min, 1000 rpm), 200 µl of solution was collected each into two Eppendorf tubes for LDH content to be tested.

The level of LDH secreted from the tested samples was analysed. The LDH assay was performed according to the manufacturer's protocol (CytoTox 96® Non-Radioactive Cytotoxicity Assay, G1780, Promega Corporation, Madison, WI, USA) and Cobas Integra analyser (ROCHE).

Selected samples subjected to laser nanostructuring (B372\_30 2 mm/s, B372\_30 10 mm/s) were examined for cellular growth. For this purpose, the samples were placed in an autoclave at 135°C and 2.1 bar pressure. Tests were performed on Normal Human Dermal Fibroblasts (NHDF, Promocell, Germany) C-12302. Fibroblast Growth Medium 2 Ready-to-use (C 23010, PromoCell, Germany) was used as the culture medium enriched with Supplement Mix (C-39315, PromoCell, Germany) and Antibiotic Antimycotic Solution (A5955, Sigma Aldrich, USA).

Cells were cultured for 96 h, after which they were washed to remove any residual culture medium and non-adsorbed proteins. This process was similar to that used in direct cytotoxicity tests, followed by incubation with fluorescent dyes that enable the assessment of cell viability and mitochondrial activity.

For samples subjected to laser nanostructuring, cytotoxicity studies were no longer conducted. Instead, analyses of cell behaviour were carried out at the three marked locations in the diagram according to FIG. 1. Two types of staining were applied, which are techniques used mainly in cell biology and microscopic studies, allowing the examination of various structures within cells. Each of these dyes serves a specific purpose and enables visualization of different elements of the cell:

**ALEXA + DAPI:** Alexa 488 is primarily used for labelling proteins in cells. It is frequently applied to specifically detect selected proteins or structures within the cell, in this case, labelling receptors and cytoskeletal proteins (e.g. actin). The conjugate labelled with Alexa 488 used for cell staining is Alexa Fluor 488 phalloidin, which is conjugated with the Alexa 488 fluorescent dye and specifically binds to F-actin in the cytoskeleton. Staining with Alexa Fluor 488 and DAPI allows for simultaneous visualization of proteins and cell nuclei. It is mainly used to study cell structure and function, analyse their distribution, number, and protein interactions in the context of cell morphology. This technique is invaluable in studies of cell biology and processes such as apoptosis or cell migration.

**FAK100:** This technique allows simultaneous analysis of protein organization in cells using Alexa Fluor, nuclear localization and cell state through DAPI, and adhesion connections and cellular signalling via FAK 100. The entire process serves to study cell interactions with their environment, analyse the cytoskeleton, and monitor cell migration and growth, which is key in studies on cancer development, cell differentiation, and their response to environmental stimuli. For each modification, images were taken at three locations on the sample. The images were captured using the same procedure as for digital microscopy, following the established protocol.

#### **Protein biofilm formation and hemocompatibility test**

The whole human blood was obtained from the Regional Donation Centre (Krakow, Poland) containing sodium citrate anticoagulant based on the official contract signed and the appropriate permits issued. The agreement was signed between the Institute of Metallurgy and Materials Science of the Polish Academy of Sciences in Krakow and the Regional Center for Blood Donation on 5.07.2024 and is valid until 4.07.2027. Prior to experiments, the control for platelet activation was prepared by blood activation with adenosine diphosphate (ADP, 20 µM final concentration) for 10 min. Samples placed in multi-well dishes gently stirred on a laboratory cradle, ensuring a constant and continuous flow over the surface for 20 min (laboratory cradle for 20 min). In this case, a laboratory cradle refers to a device or platform designed to hold blood samples securely during testing. This equipment ensures stability and minimizes movement, which is critical for accurate measurements and observations, particularly when analysing blood properties or conducting assays. Studies on the effect of surface potential to bleach were analysed by incubating the surfaces pre-incubating in FBS (10 times resuspended 1.5 mL) for 2 h and whole blood (1.5 mL) 20 min respectively with gentle agitation on a cradle (FBS for 2 h + laboratory cradle for 20 min). After the first incubation in FBS, the surfaces were washed with PBS and analysed for interaction with whole blood again stirring gently on the laboratory cradle for 20 min. The third type of analysis involved incubating the surfaces in whole blood for 20 min on the cradle instead of pre-incubating in FBS. After this, the surfaces were washed and then incubated again in whole blood for another 20 min on the cradle (Laboratory cradle for 20 min + Laboratory cradle 20 min). Using FBS instead of human serum helps to standardize the pre-incubation process while ensuring that the biological activity required for hemocompatibility assessment is maintained. Serum is a part of blood plasma that is devoid of clotting factors and fibrinogen, a key protein necessary for blood clot formation. In simple terms serum is not capable of clotting. The concept behind the experiment was to create a so-called pseudointima, that has an impact on the clotting process. Due to the lack of availability of human serum, animal serum was used for the study due to its basic nature.

After the set time, blood was collected and mixed with fluorescently labelled antibodies. A 36 µL of antibodies mix was added to the bottom of the well (FITC Mouse Anti-Human CD62P, catalog number 555523, BD Biosciences, Poland; BD™ CD45 PerCP, catalog number 345809, BD Biosciences, Poland; BD Pharmingen™ PE Mouse Anti-Human CD42b (vWF), catalog number 555473, BD Biosciences, Poland). Then, 4 µL of blood taken from the sample was added. After 15 min, a blood sample was blocked with 400 µL FBS and, after 10 min, fixed with 3.5 mL cold 1% formalin solution dissolved in PBS.

The elaborated blood samples 35  $\mu\text{L}$  were dotted and spread on a poly-L-lysine slide and covered with a cover slip. The analysis was performed on confocal laser scanning microscopy (CLSM Exciter 5 Axiolmager, Zeiss). The fluorescent analysis of the blood activation on the surface was done on CLSM.

## Results and Discussions

### Surface topography

The optical observations obtained by digital microscopy and the surface topography parameters of the analysed samples with ALD coating are presented in FIG. 2 and FIG. 3, respectively.

Based on the microscopic images, distinct differences in the surface topography between the uncoated samples and those with the ALD coating can be observed. The roughness parameters are noticeably lower for the samples with the ALD coating compared to the unmodified substrates. The heterogeneous surface observed in FIG. 2 after ALD coating may result from variations in thickness or texture due to the deposition process. Despite this heterogeneity, the overall roughness parameters can decrease, as the ALD coating may fill in surface features, leading to a smoother average profile. Thus, while the surface appears varied at a microscale, the statistical analysis over a larger area shows reduced roughness values. This reduction in roughness could be attributed to the uniform deposition of the ALD layer, which smooths out surface irregularities and creates a more homogeneous surface. The coating likely fills in microscopic valleys and smoothens peaks, leading to an overall decrease in surface roughness.

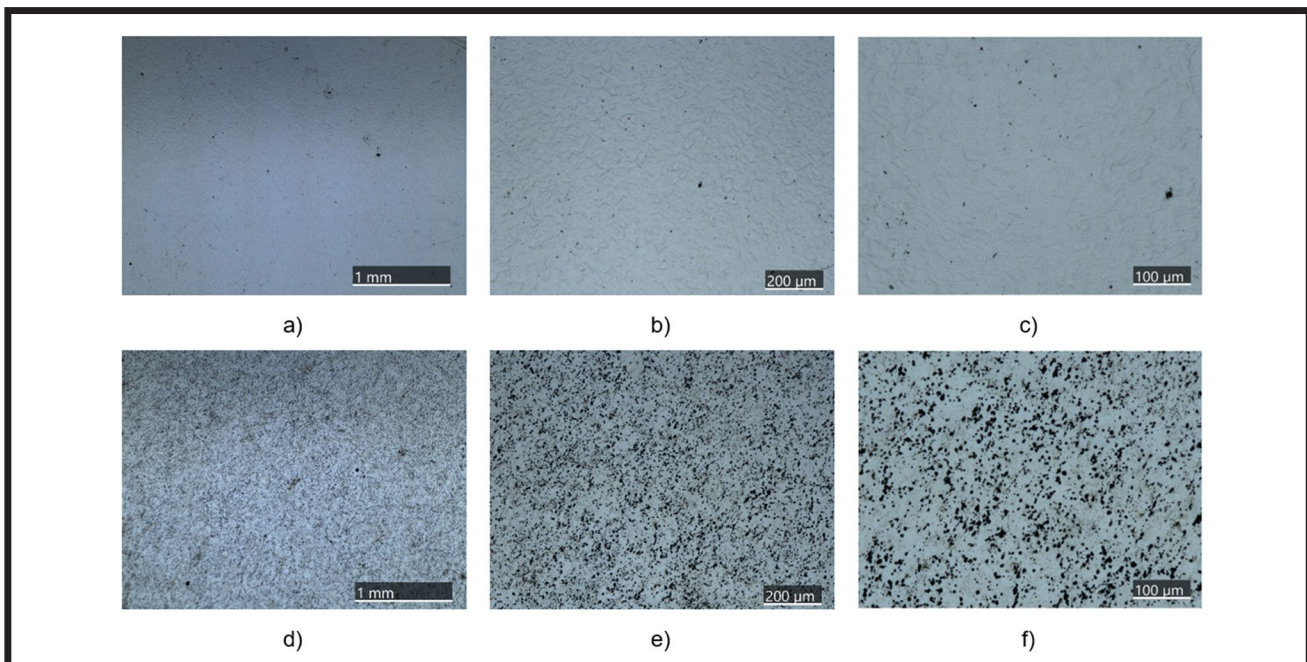


FIG. 2. Surface topography: a) Nitinol surface 100 x; b) Nitinol surface 300 x; c) Nitinol surface 600 x; d) Nitinol surface with ALD coating 100 x; e) Nitinol surface with ALD coating 300 x; f) Nitinol surface with ALD coating 600 x.

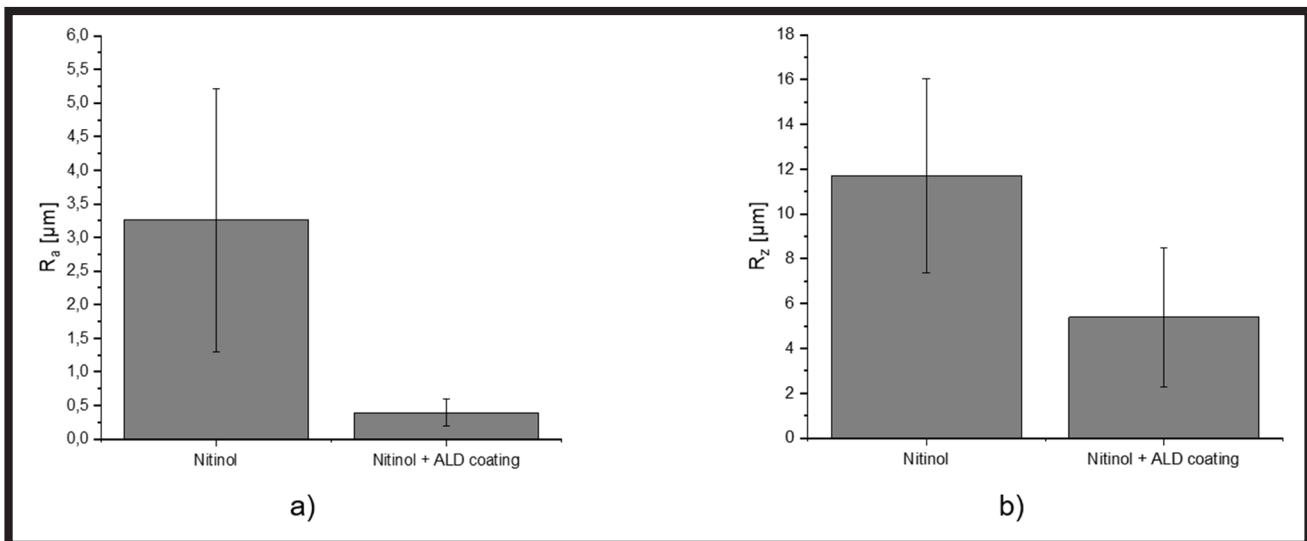


FIG. 3. Roughness parameters on the sample: a)  $R_a$  (average roughness); b)  $R_z$  (average maximum height of the profile).

The surface appearance was illustrated using a representative sample, where channels were made using laser technology with a beam travel speed of 10 mm/s. A single sample was selected because, in all cases, the channels were made as radially propagating lines. The optical observations gained by the digital microscopy of the analysed samples after laser nanostructuring are presented in FIG. 4. The profile of the processed images was performed by ConfoMap software. The images illustrate the shape of the channels – profile (FIG. 4d, 4h, 4l) according to the red lines from FIG. 4a, 4e, 4j).

FIG. 5 presents a comparison of surface roughness for B372\_29 samples, considering two extreme cutting speeds: 2 mm/s and 10 mm/s.

For this study, two extreme samples were presented: one with the lowest drilling speed (2 mm/s) and one with the highest drilling speed (10 mm/s).

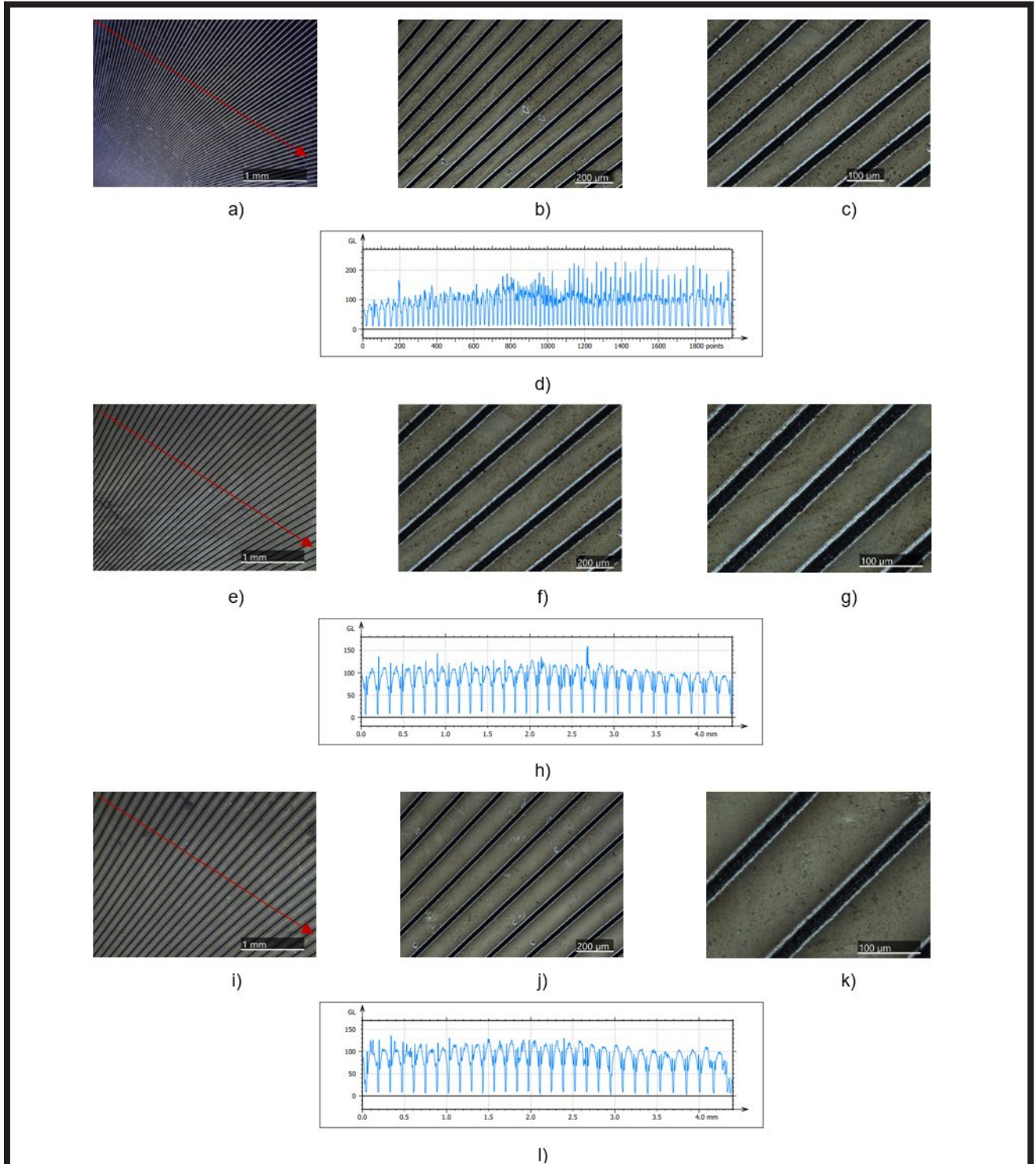


FIG. 4. Surface topography in characteristic places on the sample after laser nanostructuring B372\_29 10 mm/s: a) BEGINNING 100 x; b) BEGINNING 300 x; c) BEGINNING 600 x; d) BEGINNING 100 x – profile; e) MIDDLE 100 x; f) MIDDLE 300 x; g) MIDDLE 600 x; h) MIDDLE 100 x – profile; i) END 100 x; j) END 300 x; k) END 600 x; l) END 100 x – profile.



Based on microscopic analyses, it was observed that at the beginning of the channels elaborated, they were positioned closer together than at the end, where these channels are further apart. As the distance between the channels increases, their dimensions also become larger. These changes were further confirmed by the topographic profile, which shows how the size and spacing of the channels gradually change along the sample.

The roughness parameters, such as  $R_a$  and  $R_z$ , decreased simultaneously with increasing distance between the channels. The channels in the BEGINNING area (FIG. 1) were characterised with greater topographical variation comparing to the channels analysed in MIDDLE and END areas (FIG. 1). The observed decrease in the roughness parameters may prove the improvement of the homogeneity of the topography.

### Contact angle analysis and surface free energy

The results of the contact angle measurement are presented in FIG. 6. In the case of samples modified by laser nanostructuring, the values of the contact angle and SFE were not analysed due to the fact that the laser grooves were drilled in a radial manner rather than parallel, so contact angle measurements may be inadequate. The laser-cut grooves introduce changes in topography, leading to variations in wettability properties across different areas, which complicates the interpretation of the results. The grooves can affect the movement of liquids, resulting in a misleading representation of the material's wettability, with results potentially differing depending on the direction and depth of the grooves. Measuring the contact angle on uneven surfaces can be technically challenging, introducing additional measurement errors. For these reasons, contact angle studies may not be effective in assessing the wettability properties of materials with laser-cut grooves.

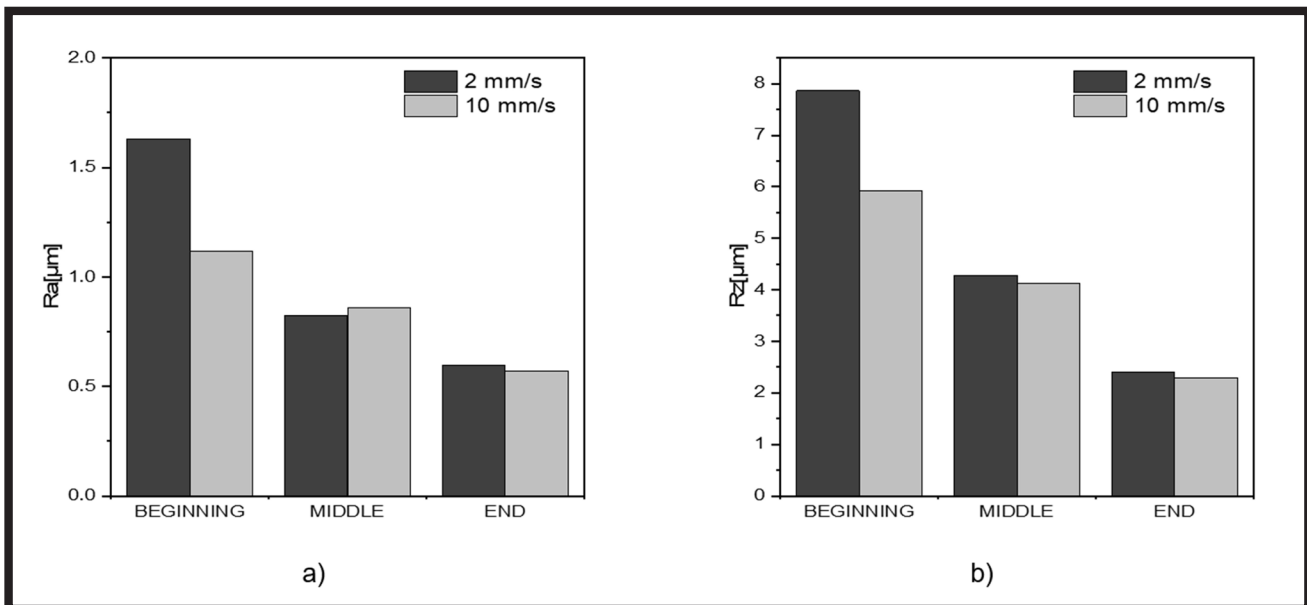


FIG. 5. Roughness parameters in the characteristic places on the sample B372\_29: a)  $R_a$  (roughness average); b)  $R_z$  (average maximum height of the profile).

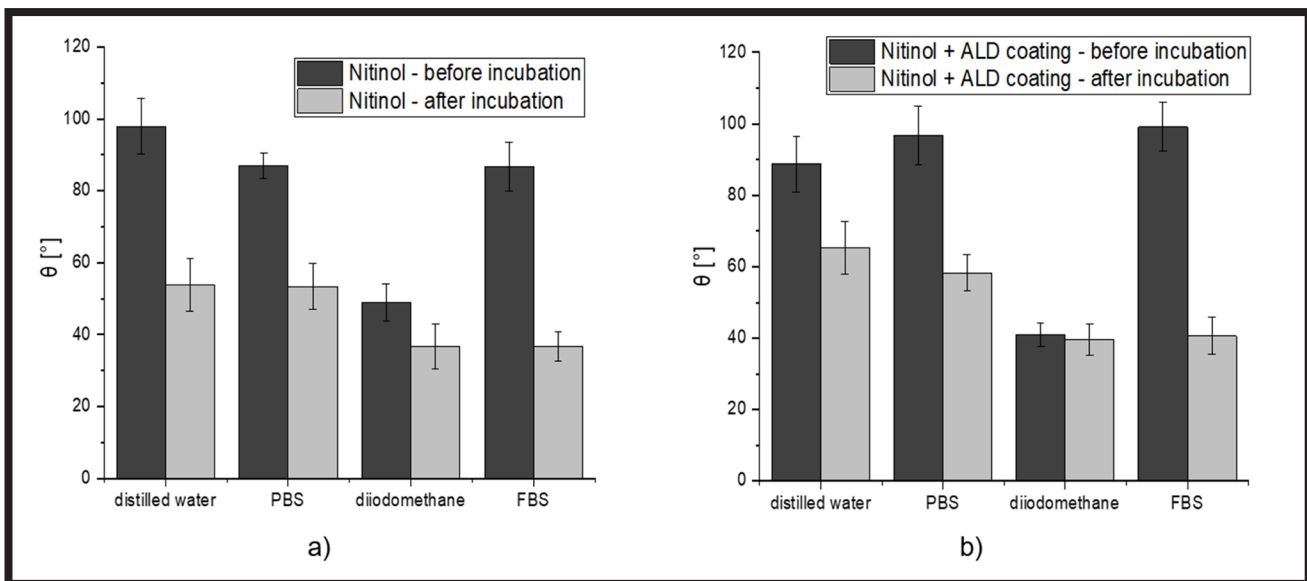


FIG. 6. Contact angle values: a) Nitinol alloy surface before and after incubation in FBS; b) Nitinol alloy with ALD coating surface before and after incubation in FBS.

**TABLE 3. Components of surface free energy calculated by Owens-Wendt model.**

| Type of sample                            | SFE | $\gamma_s$<br>[mJ/m <sup>2</sup> ] | $\gamma_s^d$<br>[mJ/m <sup>2</sup> ] | $\gamma_s^p$<br>[mJ/m <sup>2</sup> ] |
|---|-----|------------------------------------|--------------------------------------|--------------------------------------|
| Nitinol – before incubation               |     | 35.13                              | 34.84                                | 0.29                                 |
| Nitinol + ALD coating – before incubation |     | 40.36                              | 39.10                                | 1.26                                 |
| Nitinol – after incubation                |     | 56.45                              | 41.24                                | 15.21                                |
| Nitinol + ALD coating – after incubation  |     | 49.43                              | 39.83                                | 9.60                                 |

Surface free energy was determined by using the Owens-Wendt model (TABLE 3).

The contact angles for Nitinol and Nitinol with ALD coating change after incubation in 10 X FBS, suggesting that both the material and the coating undergo certain surface modifications as a result of incubation.

For Nitinol (without ALD coating), the contact angle for distilled water decreases from 97.9° to 53.9°, indicating an increase in the surface hydrophilicity after the incubation process. A similar trend can be observed for other liquids, for example, PBS (a decrease from 86.9° to 53.4°), diiodomethane (from 49.0° to 36.7°), and FBS (from 86.7° to 36.6°). For Nitinol with ALD coating, the decrease in the contact angle after incubation is less pronounced, especially for distilled water (from 88.7° to 65.3°), which suggests that the ALD coating protects the surface from drastic changes in hydrophilicity. However, some change still occurs, which can be interpreted as the surface's response to incubation conditions.

The ALD coating influences the surface properties, making it more hydrophilic. However, after incubation, the differences in contact angles are smaller, suggesting that the coating protects the surface but does not entirely prevent changes in wettability. In most instances, Nitinol with ALD coating shows smaller changes in contact angles after incubation compared to Nitinol without the coating, which may indicate that the coating stabilizes the material's surface.

The ALD coating increases the total surface free energy and slightly improves the material's hydrophilicity, which may positively affect interactions with the biological environment. It is also more stable in contact with the incubation medium, as the changes after incubation are less drastic compared to uncoated Nitinol. The uncoated material after incubation shows significantly greater changes in both total SFE and its polar component, which may indicate higher surface reactivity to the environment.

### Cell-material interaction analysis

Cell viability on Nitinol and Nitinol alloy with ALD coating samples was assessed after 48 h of incubation using fluorescence staining and confocal microscopy (FIG. 7).

Based on the confocal microscopy images, a similar number of cells was observed both for the reference material and the material modified with SiO<sub>2</sub>. According to the ISO 10933-5 standard, the degree of cytotoxicity can be considered weak, because no more than 20% of cells are rounded, shrunken, and only single cells are damaged.

The results from the LDH assays of the samples after direct cytotoxicity testing and testing on extracts are presented in FIG. 8. These analyses provide insight into the cellular response and potential cytotoxic effects of the modified surfaces.

For the direct cytotoxicity tests, the results for the unmodified sample and the sample with coatings are at similar levels, which are also comparable to the control sample (PS). Based on the results of the LDH analysis (FIG. 8) from cytotoxicity testing performed on extracts, a similar level of LDH was observed for subsequent samples, both for 24 and 48 h. An increase in the LDH level was observed for the 9:1, 48 h sample (Nitinol surface + coating).

Cell growth studies were conducted on samples indicated as B372\_29 2 mm/s (FIG. 9) and B372\_29 10 mm/s (FIG. 10). The first set, Alexa Fluor 488 and DAPI, stained the actin cytoskeleton (green) and cell nuclei (blue), respectively. The second set, FAK-100, consisted of three dyes: phalloidin conjugated with TRITC, anti-vinculin, and DAPI. This set stained structures such as actin fibres in the cytoskeleton (red), adhesive molecules (green), and cell nuclei (blue) in accordance with the representations shown in FIGs. 9 and 10. For each modification, images were taken at three locations on the sample according to FIG. 1.

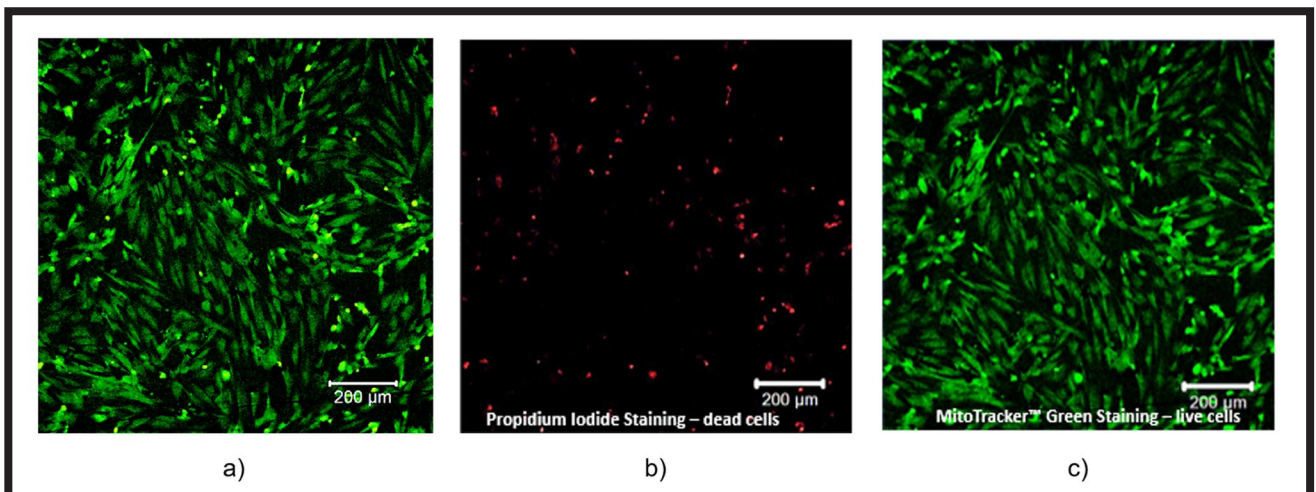


**FIG. 7. FDA + PI staining Nitinol + ALD deposited coating: a) FDA + PI staining; b) separated channel for PI staining – dead cells; c) separated channel for FDA staining – live cells.**



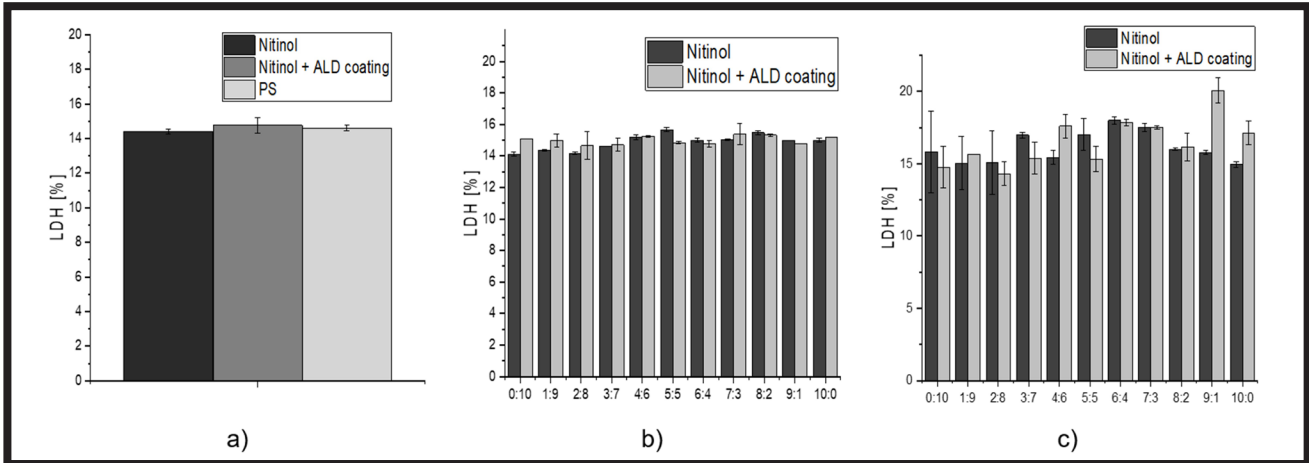


FIG. 8. Analyses of LDH after: a) direct cytotoxicity; b) on extracts after 24 h incubation; c) on extracts after 48 h incubation.

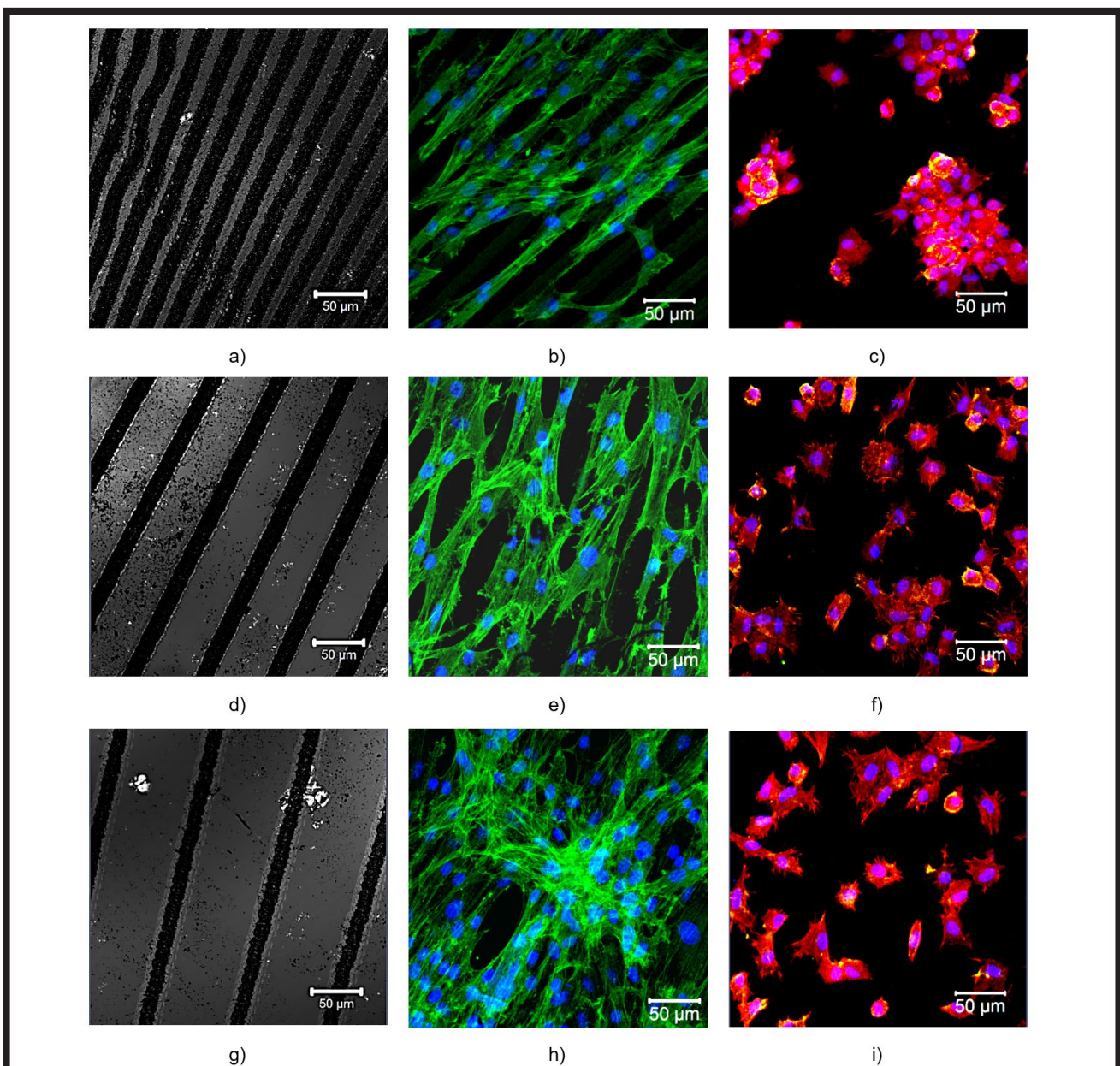
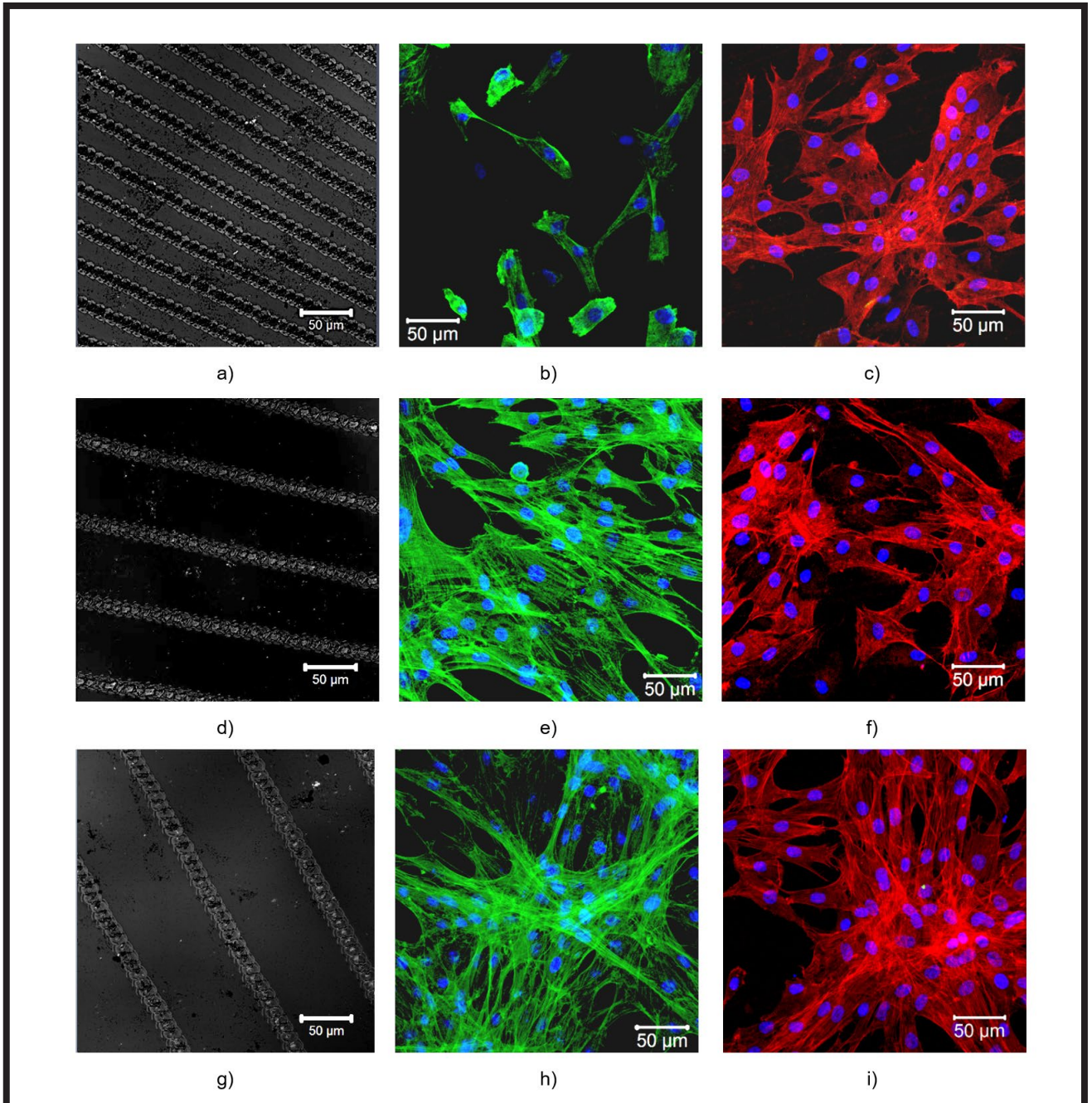


FIG. 9. B372\_29 2 mm/s: a) topography: BEGINNING; b) ALEXA + DAPI: BEGINNING; c) FAK100: BEGINNING; d) topography: MIDDLE; e) ALEXA + DAPI: MIDDLE; f) FAK100: MIDDLE; g) topography: END; h) ALEXA + DAPI: END; i) FAK100: END.



**FIG. 10.** B372\_29 10 mm/s: a) topography: BEGINNING; b) ALEXA + DAPI: BEGINNING; c) FAK100: BEGINNING; d) topography: MIDDLE; e) ALEXA + DAPI: MIDDLE; f) FAK100: MIDDLE; g) topography: END; h) ALEXA + DAPI: END; i) FAK100: END.

The results obtained from the studies on laser nanostructuring of samples indicate significant differences in the morphology of migratory channels depending on the cutting speed. Analysis of topographic images reveals that at a speed of 10 mm/s, the channels exhibit serrated, less precise edges, compared to laser cut channels at a lower speed, which may influence the way cells interact with their environment. In contrast, at a speed of 2 mm/s, the channels are characterized by wider, less defined edges, potentially facilitating a more flexible adaptation of cells to their shape.

Actin/nuclei staining shows that the cytoskeleton of the cells adopts the shape of the channel, suggesting a dynamic adaptation of cells to spaces with variable geometry. It is noticeable that cells grow within these structures of the channel.

Actin cytoskeleton, adhesive molecules and cell nuclei were stained using the FAK-100 kit. It indicates a high dynamic network of actin cytoskeleton, a substantial presence of the actin cytoskeleton was observed; however, these cells exhibit a limited number of adhesion molecules. This condition may arise from the fact that a more developed cytoskeleton, responsible for mechanical strength and migratory capacity, does not correlate with high expression of adhesion molecules. Based on the staining analysis, it can be concluded that the number of cells on the examined surfaces is significant, suggesting that the material supports cell adhesion. However, their flattened morphology indicates that they may be in a state of proliferation or active migration. Weak interactions between the cells and the material may be due to insufficient amounts of adhesive molecules. The low presence of these molecules can limit the cells' ability to adhere properly.



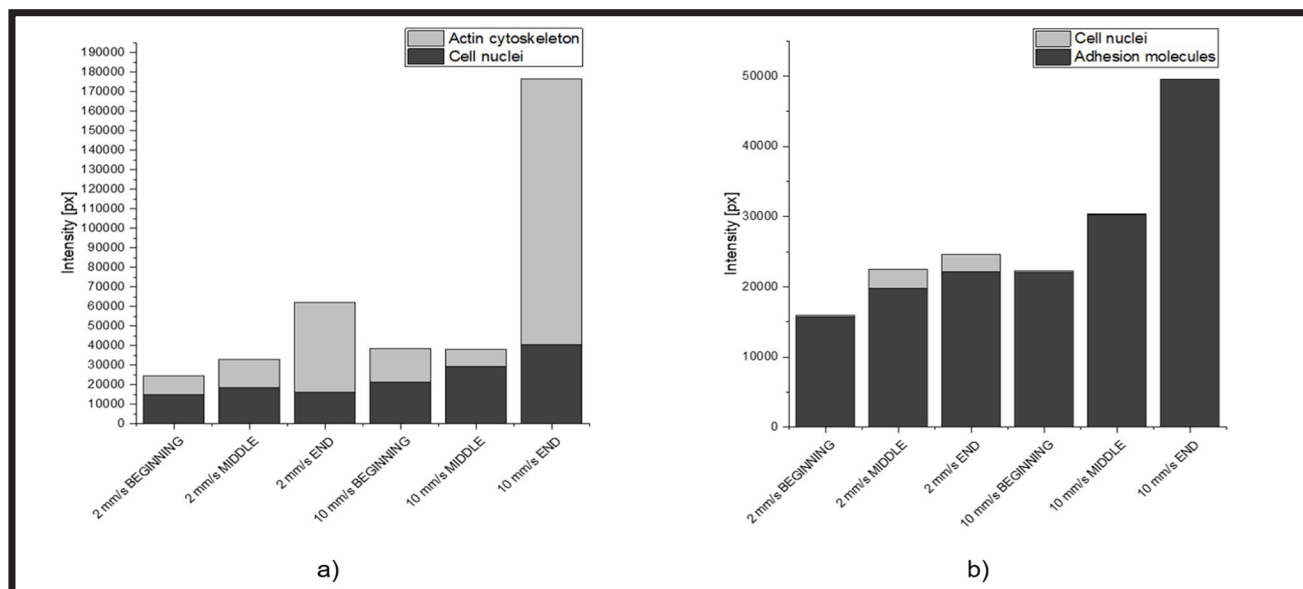


**FIG. 11. Colocalization of FAK-100 staining: a) red to blue channel ratio (vinculin to DAPI); b) green to blue channel ratio (adhesion molecules to DAPI).**

The analysis quantitatively examined the FAK 100 using colocalization for: vinculin to DAPI ratio and adhesion molecules to DAPI ratio is shown in FIG. 11. This approach was utilized to assess the spatial distribution and interaction between these proteins and the cellular structures, providing insight into their role in cellular processes.

This type of analysis does not require the calculation of statistical error as it deals with the relationship between one set of values and another. The data are comparative rather than measuring dispersion within a single set of values. Therefore, the results of the analysis can be interpreted without the need for statistical measures of error.

The results of the colocalization analysis of FAK-100 staining reveal significant insights into the interaction between the cytoskeleton and the cell nuclei, depending on the laser cutting speed. A similar ratio of nuclei to cytoskeleton is observed under different conditions; however, for the sample at 2 mm/s, there is twice as much cytoskeleton relative to the nuclei, while at 10 mm/s, the ratio of cytoskeleton to nuclei increases several times.

This difference may be attributed to changes in the morphology of the channels caused by the laser cutting speed. In comparison to the 10 mm/s, at 2 mm/s, the wider and less defined edges of the channels may facilitate a more favourable interaction between the cytoskeleton and the substrate, supporting the development of the cytoskeletal network. The increased presence of the cytoskeleton may enhance cell stability and facilitate migration as cells adapt to the geometry of the channels. In contrast, at a speed of 10 mm/s, the serrated and less precise edges of the channels compared to 2 mm/s likely hinder the establishment of stable cytoskeletal connections. The increased presence of the cytoskeleton relative to the nuclei in this case suggests the cells may be attempting to strengthen their mechanical resilience in response to suboptimal conditions.

The analysis of adhesion molecules reveals a substantial presence of nuclei alongside a lack of adhesion molecules. This may suggest that, despite the high cell density, their ability to adhere to the substrate and to each other is limited. The predominance of nuclei may indicate that, despite the high number of cells, they are unable to effectively interact with their environment due to low expression of adhesion molecules. The absence of stable connections may restrict their migratory and proliferative capabilities.

### Hemocompatibility test

After blood-material interaction tests, the smear samples were stained and imaged using CLSM (FIG. 12). The images were normalized to the fluorescence intensity of the ADP reference sample to ensure consistent comparison across samples and to account for variations in the fluorescence signal that may arise from experimental conditions. The results are categorized by samples and the types of analyses performed.

Based on the CLSM observations, no activation of the coagulation system was observed in tests using blood. A significant increase in platelet count was observed for samples initially incubated in FBS and subsequently in blood compared to samples incubated on the laboratory cradle for 20 min and samples initially incubated in blood instead of FBS. The preincubation in FBS aimed to create a protein layer on the surface of the samples, which could have promoted greater platelet adhesion after the blood was applied. The protein layer formed by FBS may have acted as an interface between the biomaterial surface and the blood, influencing cell behaviour and their interaction with the surface.

Reduced presence of von Willebrand factor (vWF) in all samples was observed, which can be considered a favourable outcome. The vWF was detected using the BD Pharmingen™ PE Mouse Anti-Human CD42b antibody. High levels of vWF could indicate the activation of pro-thrombotic processes, while the reduced amount of vWF suggests that the surface modifications effectively reduced the risk of thrombogenicity, which is a positive aspect in terms of biocompatibility. High platelet counts were observed in all samples, with the most significant values noted for those incubated in FBS before exposure to blood. In the case of Nitinol samples with an ALD coating and a sample with a laser speed of 2 mm/s, blood preincubation also resulted in a higher platelet count compared to other samples. This suggests that the modification favoured the interaction with blood. The results indicate that the modified biomaterial surfaces, especially those incubated in FBS, promote platelet adhesion while not triggering a clear activation of the coagulation cascade. The analysis quantitatively examined the hemocompatibility test using colocalization for: vWF to fibrinogen, CD62P to vWF, CD62P to fibrinogen are shown in FIG. 13.



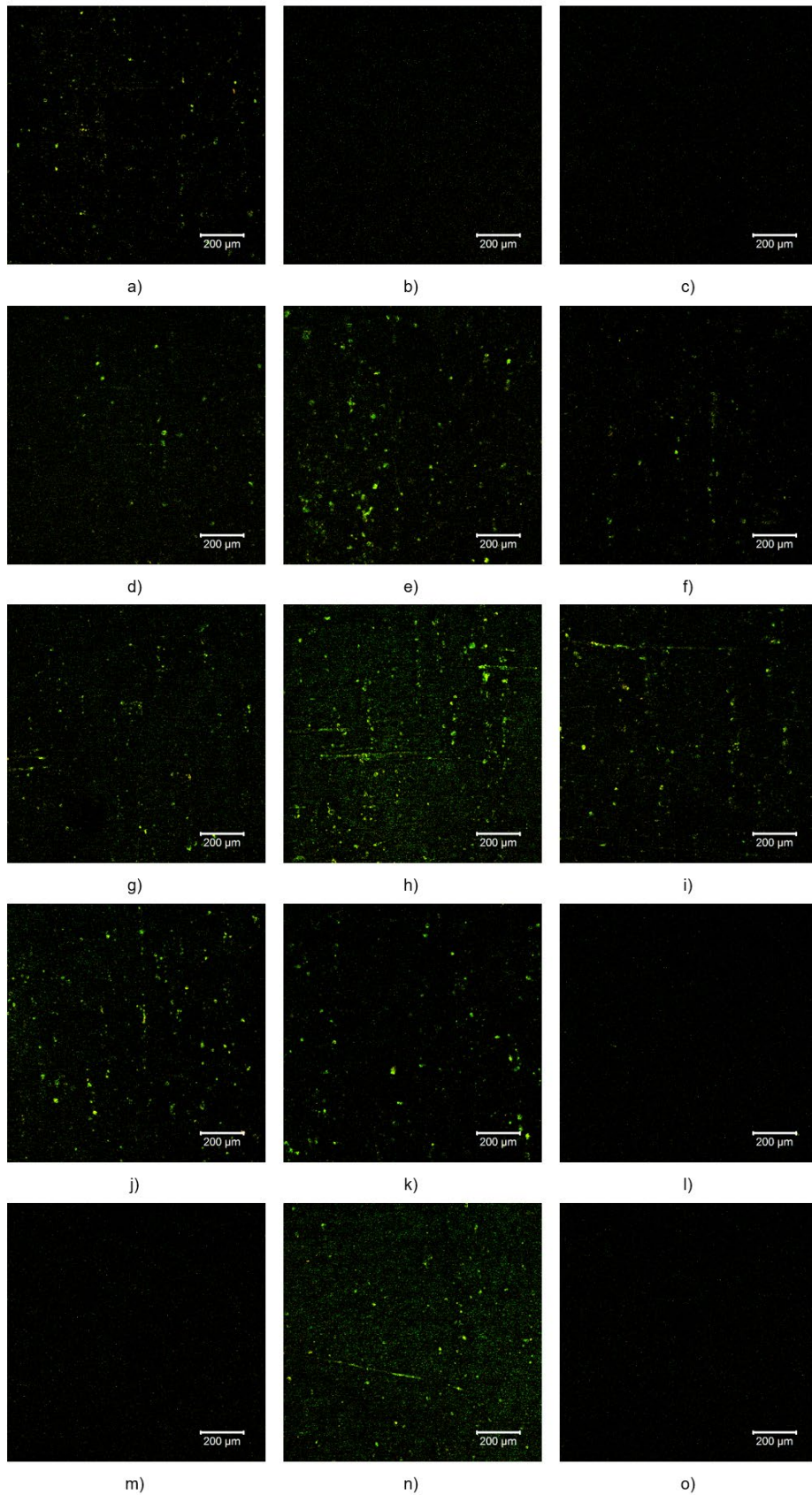


**FIG. 12. Confocal microscopy analysis concerning blood-material interaction: a) Nitinol – laboratory cradle; b) Nitinol – FBS + laboratory cradle; c) Nitinol – laboratory cradle x2; d) Nitinol with ALD coating – laboratory cradle; e) Nitinol with ALD coating – FBS + laboratory cradle; f) Nitinol with ALD – laboratory cradle x2; g) B372\_26 2 mm/s – laboratory cradle; h) B372\_26 2 mm/s – FBS + laboratory cradle; i) B372\_26 2 mm/s – laboratory cradle x2; j) B372\_26 6 mm/s – laboratory cradle; k) B372\_26 6 mm/s – FBS + laboratory cradle; l) B372\_26 6 mm/s – laboratory cradle x2; m) B372\_26 8 mm/s – laboratory cradle; n) B372\_26 8 mm/s – FBS + laboratory cradle; o) B372\_26 8 mm/s – laboratory cradle x2.**

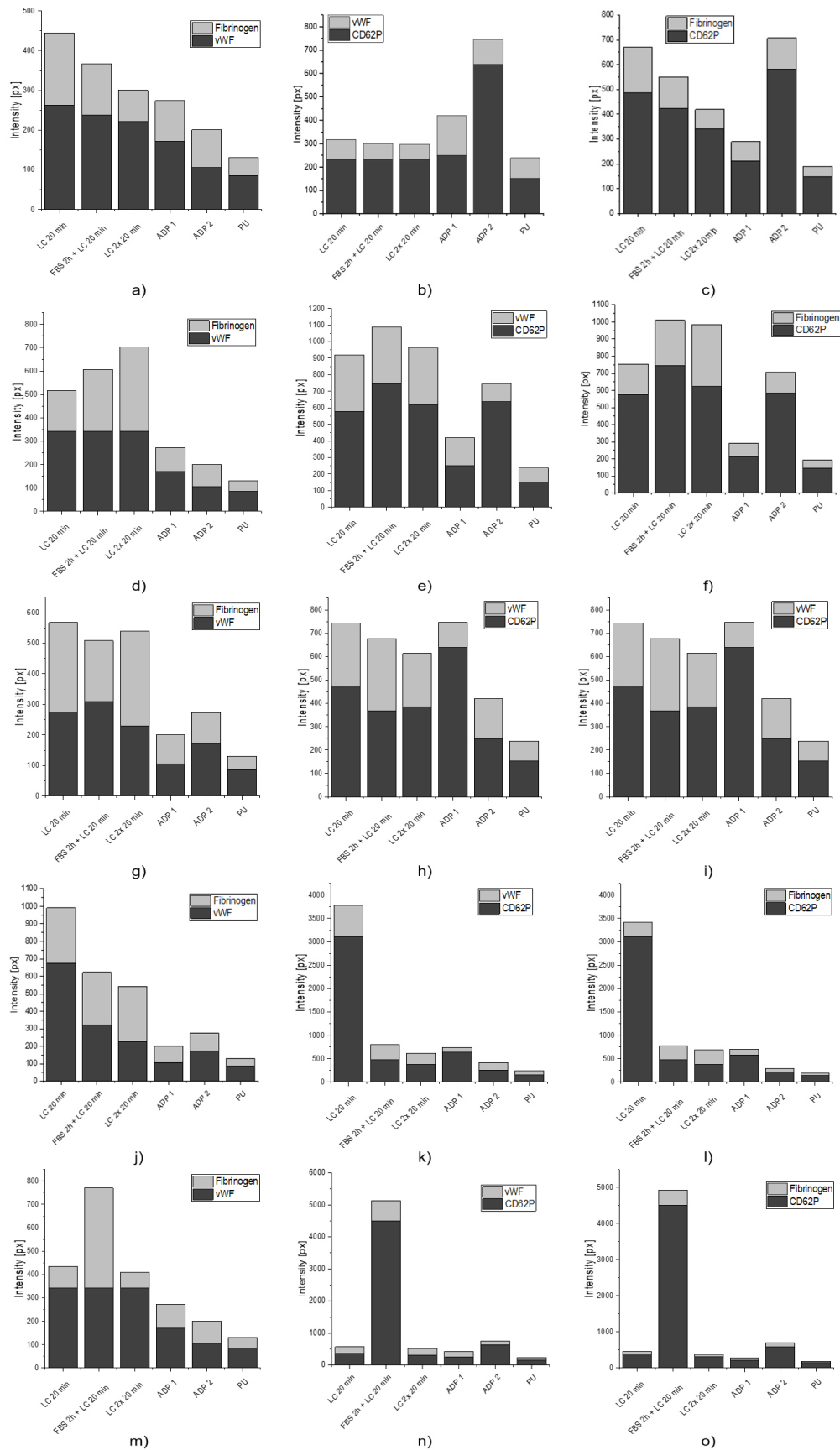


FIG. 13. Colocalization of blood-material interaction: a) Nitinol – vWF to fibrinogen; b) Nitinol – CD62P to vWF; c) Nitinol – CD62P to fibrinogen; d) Nitinol with ALD coating – vWF to fibrinogen; e) Nitinol with ALD coating – CD62P to vWF; f) Nitinol with ALD – CD62P to fibrinogen; g) B372\_26 2 mm/s – vWF to fibrinogen; h) B372\_26 2 mm/s – CD62P to vWF; i) B372\_26 2 mm/s – CD62P to fibrinogen; j) B372\_26 6 mm/s – vWF to fibrinogen; k) B372\_26 6 mm/s – CD62P to vWF; l) B372\_26 6 mm/s – CD62P to fibrinogen; m) B372\_26 8 mm/s – vWF to fibrinogen; n) B372\_26 8 mm/s – CD62P to vWF; o) B372\_26 8 mm/s – CD62P to fibrinogen.

This type of analysis does not require the calculation of statistical error, as it deals with the relationship between one set of values and another. The data are comparative rather than measuring dispersion within a single set of values. Therefore, the results of the analysis can be interpreted without the need for statistical measures of error.

Colocalization of fibrinogen with vWF (FIG. 13a) and CD62P with vWF and fibrinogen (FIG. 13b, 13c) shows moderate signal intensity, which suggests that the interactions between markers are present but relatively mild. This may indicate moderate platelet activation and the initial stages of the coagulation response.

For samples coated with ALD, a higher signal intensity of colocalization was observed compared to samples without the coating. This applies to the colocalization of vWF with fibrinogen (FIG. 13d) as well as CD62P with vWF and fibrinogen (FIG. 13e, 13f). These results suggest that the ALD coating may enhance the interaction between the blood and the material surface, leading to greater activation of the coagulation system.

The results for B372\_26 samples subjected to laser speeds of 2 mm/s, 6 mm/s, and 8 mm/s show varying intensities of colocalization signals. Higher laser speeds during groove cutting increased the signal intensity, suggesting that higher laser speeds lead to more pronounced interactions between the coagulation markers (vWF, fibrinogen, CD62P) and the material surface. For example, the colocalization of vWF with fibrinogen and CD62P with fibrinogen at 2 mm/s (FIG. 13g, 13h, 13i) is less intense compared to the results for 8 mm/s (FIG. 13m, 13n, 13o), where the colocalization signals are the strongest.

In summary, the results suggest that both the application of an ALD coating and the higher laser speeds during groove formation on the Nitinol surface may intensify platelet activation, which is crucial for designing implants with optimized biocompatibility.

Regarding the presence of fibrin, its quantity was relatively low, indicating that the full activation of the coagulation cascade did not occur. This suggests the absence of significant coagulation initiation, another positive result, indicating that the modified biomaterial surfaces did not provoke a strong pro-thrombotic response.

## Conclusions

The biocompatibility of Nitinol is significantly influenced by its surface characteristics [6-9]. The results indicate a reduction in roughness due to ALD coating, which aligns that smoother surfaces generally promote better endothelialization and reduce thrombus formation. The topographical modifications through laser nanostructuring can enhance cellular interactions [8,9]. Smoother, more defined edges resulting from lower laser cutting speeds (2 mm/s) are likely to facilitate cell migration and adhesion, which is crucial for integrating implants into the cardiovascular system. In contrast, the less defined edges at higher speeds may hinder stable cellular interactions, as noted in the results of our staining analyses.

The reduced levels of von Willebrand factor (vWF) result in a lower risk of thrombus formation, which is particularly beneficial for devices that come into direct contact with blood in the long-term success of devices such as atrial septal defect (ASD) occluders. This observation is crucial when considering the clinical application of modified Nitinol surfaces in transcatheter closure devices and other cardiovascular implants.

In conclusion, integrating our results with existing literature underscores the critical role of surface chemistry and topography in determining the biocompatibility of Nitinol for cardiovascular applications. This provides a comprehensive understanding of how topographical and chemical modifications influence the material's performance in blood-contacting environments. Based on the results, an analysis of the impact of surface modifications and laser nanostructuring on the properties of biomaterials was conducted. The following conclusions were formulated:

The ALD coating significantly reduced the roughness parameters compared to the unmodified samples. Uniform deposition of the ALD layer smoothed the surface, creating a more homogeneous topography.

After incubation in FBS, both Nitinol samples and those with the ALD coating exhibited increased hydrophilicity. The ALD coating limited changes in hydrophilicity, suggesting its protective role in stabilizing surface properties and preventing drastic shifts in wettability. The ALD coating acts as a stabilizer, limiting changes and reducing the increase in polarity, suggesting it is more resistant to chemical modifications caused by incubation.

A slower laser cutting speed (2 mm/s) resulted in channels with smoother and wider edges, promoting better cell adaptation and migration. In contrast, faster cutting (10 mm/s) led to serrated, less-defined edges, which may hinder stable cell attachment.

Cells dynamically adapted their cytoskeleton to the geometry of laser-created channels, especially at slower cutting speeds. The surface topography influenced cell migration and their mechanical interactions with the substrate.

The samples exhibited low cytotoxicity, with no significant increase in LDH levels, confirming their biocompatibility. Moreover, no activation of the coagulation system was observed in blood interaction tests, indicating the suitability of these surface modifications for medical applications.

## Acknowledgements

*The project was funded by the National Science Centre, Poland, allocated on the basis of the decision No. 2023/49/B/ST11/03301. Part of the research was done as a part of the statutory activities of the Institute of Metallurgy and Materials Science PAS-Z-8.*



## References

- [1] M.J. Van Ligten, D.E. Rappaport, L.B. Querin, W.A. Martini: Atrial Septal Defect (ASD) Repair Unveiling an Unusual Conduction Conundrum: A Wenckebach Case Report., *Cureus* 16 (2024) e62073. <https://doi.org/10.7759/cureus.62073>.
- [2] G. Fischer, J. Stieh, A. Uebing, U. Hoffmann, G. Morf, H.H. Kramer: Experience with transcatheter closure of secundum atrial septal defects using the Amplatzer septal occluder: a single centre study in 236 consecutive patients. *Heart* 89 (2003) 199-204. <https://doi.org/10.1136/heart.89.2.199>.
- [3] S. Shrivastava, S. Shrivastava, S.V.V. Allu, P. Schmidt: Transcatheter Closure of Atrial Septal Defect: A Review of Currently Used Devices. *Cureus* 15 (2023) e40132. <https://doi.org/10.7759/cureus.40132>.
- [4] T. He, J. He, Z. Wang, Z. Cui: Modification strategies to improve the membrane hemocompatibility in extracorporeal membrane oxygenator (ECMO). *Adv Compos Hybrid Mater* 4 (2021) 847-864. <https://doi.org/10.1007/s42114-021-00244-x>.
- [5] R. Fiszer, M. Chojnicki, A. Sukiennik, I. Świątkiewicz, M. Woźnicki: Embolizacja prawej komory zestawem Amplatza implantowanym w ubytek przegrody międzyprzedsionkowej. *Folia Cardiologica Excerpta* 2(4) (2007) 162-165.
- [6] C. Constant, S. Nichols, É. Wagnac, Y. Petit, A. Desrochers, V. Brailovski: Biocompatibility and mechanical stability of Nitinol as biomaterial for intra-articular prosthetic devices. *Materialia (Oxf)* 9 (2020) 100567. <https://doi.org/10.1016/j.mtla.2019.100567>.
- [7] M. Jenko, M. Godec, A. Kocijan, R. Rudolf, D. Dolinar, M. Ovsenik, M. Gorenšek, R. Zaplotnik, M. Mozetic: A new route to biocompatible Nitinol based on a rapid treatment with H<sub>2</sub>/O<sub>2</sub> gaseous plasma. *Appl Surf Sci* 473 (2019) 976-984. <https://doi.org/10.1016/j.apsusc.2018.12.140>.
- [8] A. Bandyopadhyay, I. Mitra, S.B. Goodman, M. Kumar, S. Bose: Improving biocompatibility for next generation of metallic implants, *Prog Mater Sci* 133 (2023) 101053. <https://doi.org/10.1016/j.pmatsci.2022.101053>.
- [9] S. Shabalovskaya, J. Anderegg, J. Van Humbeeck: Critical overview of Nitinol surfaces and their modifications for medical applications. *Acta Biomater* 4 (2008) 447-467. <https://doi.org/10.1016/j.actbio.2008.01.013>.
- [10] J.D. Hochberg, D.M. Wirth, J.K. Pokorski: Surface-Modified Melt Coextruded Nanofibers Enhance Blood Clotting In Vitro. *Macromol Biosci* 22 (2022). <https://doi.org/10.1002/mabi.202200292>.
- [11] V.S. Sotturrai, S.L. Sue, M.K. Hsu, W.K. Mann, R.C. Batson: Pseudointima formation in woven and knitted dacron grafts. A comparative ultrastructural analysis. *J Cardiovasc Surg (Torino)* 30 (1989) 808-816.
- [12] P.N. Osuchowska, R. Ostrowski, A. Sarzyński, M. Strzelec, Z. Mierczyk, E.A. Trafny: Microstructured polyethylene terephthalate (PET) for microsieving of cancer cells. *Results Phys* 15 (2019) 102612. <https://doi.org/10.1016/j.rinp.2019.102612>.